Microchim Acta (2017) 184:1315–1324
DOI 10.1007/s00604-017-2111-9

ORIGINAL PAPER

On−off−on gold nanocluster-based near infrared fluorescent probe for recognition of Cu(II) and vitamin C

Jiapeng Wu[1] · **Kaili Jiang**[1] · **Xiaojie Wang**[1] · **Chuanxi Wang**[1,2] · **Chi Zhang**[1,3]

Received: 30 August 2016 / Accepted: 27 January 2017 / Published online: 15 February 2017

Abstract The authors described gold nanoclusters (AuNCs) for use on an "on − off − on" NIR fluorescent probe for the determination of citrate and Cu(II) ion. The AuNCs were prepared by a microwave-assisted method using BSA as both the stabilizing and reducing agent. The resulting BSA-capped AuNCs display NIR fluorescence peaking at 680 nm under 500 nm excitation, a quantum yield of ~6.0%, an average size of 2.8 ± 0.5 nm, water-dispersibility, stability and biocompatibility. The on−off probe for Cu(II) is based on the interaction between Cu(II) and BSA which causes the fluorescence of the BSA−AuNCs to be quenched. The quenched fluorescence is recovered on addition of vitamin C (VC), obviously due to complexation of Cu(II) by citrate. The probe was employed to image Cu(II) and citrate in HeLa cells and in aqueous solutions. The method works in the 20 nM to 0.1 mM concentration range for Cu(II), and in the 8 nM to 120 μM concentration range for VC.

Electronic supplementary material The online version of this article (doi:10.1007/s00604-017-2111-9) contains supplementary material, which is available to authorized users.

✉ Chuanxi Wang
wangcx@nimte.ac.cn

✉ Chi Zhang
chizhang@tongji.edu.cn

[1] China-Australia Joint Research Centre for Functional Molecular Materials, School of Chemical & Material Engineering, Jiangnan University, Wuxi 214122, People's Republic of China

[2] Institute of New Energy Technology, Ningbo Institute of Industrial Technology, Chinese Academy of Sciences, Ningbo 315201, People's Republic of China

[3] School of Chemical Science and Engineering, Tongji University, 1239 Siping Road, Shanghai 200092, People's Republic of China

Keywords Nanoprobe · On-off-on probe · Fluorescence · Near-infrared · Metal nanoclusters · Imaging · HeLa cells · Microscopy · Cells

Introduction

Fluorescence-based nano-probes have attracted significant attention due to their fast response, high spatial resolution, and safety of remote handling [1, 2]. To date, various fluorescent nano-probes have been repo, including organic dyes, semiconductor quantum dots (SQDs), rare earth doped nanoparticles, carbon dots and metal nanoclusters etc. [3–7]. Compared to most other conventional fluorescent probes, near-infrared (NIR) fluorescent probes have become promising modalities for monitoring in vitro and in vivo levels of various biologically important species [8]. In general, NIR fluorophores are defined as substances that emit fluorescence in the NIR region (650–900 nm) [9]. The NIR probes with relatively high transparency and low auto-fluorescence in living tissues will provide chemists and biologists with many opportunities to conduct studies leading to a greater understanding of biological processes at the molecular level [10, 11]. At present, various kinds of NIR probes have been prepared [12, 13]. For example, protein-capped HgS SQDs with NIR emission can be used for a highly sensitive and selective sensing system for the detection of Hg^{2+} and Cu^{2+} [12]; the nanohybrids of gold nanorod and CdTe/CdS SQDs were used for turn-on fluorescent sensing of 2,4,6-trinitrotoluene(TNT) in NIR region [13]. However, these nano-probes based on heavy metals (such as Cd, and Hg) have been known to have acute and chronic toxicities, which limit their biological applications. To solve this problem, the development of new NIR nanomaterials with low toxicity to living tissues is urgently desired.

Reducing the size of metal nanoparticles down to approach the Fermi wavelength of an electron (ca. 0.5 nm for silver and gold), novel optical, electrical and magnetic properties appeared [14]. These ultra–small particles, bridging the "missing link" between atomic and nanoparticles behavior, were usually defined as nanoclusters (NCs) [15]. These metal NCs, an emerging new class of fluorescent nanomaterials have drawn increasing attention due to their unique properties and various practical applications in cell labeling, ion sensor, and catalysts [16–18]. Among them, fluorescent gold NCs (AuNCs) are attractive for a wide variety of biomedical applications, such as biosensing, in vitro and in vivo imaging, and also in cancer therapy, owing to their low toxicity, good biocompatibility and multifunctional surface chemistry [19–22]. The existing synthesis routes of fluorescent AuNCs can be divided into two groups: bottom-up and top-down methods [23, 24]. The bottom-up approach mainly based on chemical reduction of Au^{3+} ions to form metal atoms and then AuNCs appeared due to accumulation of Au atoms [23]. The $NaBH_4$, CO, N_2H_4. H2O and H_2 are usually used as reducing agents in the synthesis process through this way. However, the drawback of above methods was much complicated or time-consuming, or the low quantum yields due to the aggregation of NCs. It would be of great interest to obtain highly fluorescent AuNCs by a straightforward and effective method.

Microwave heating is considered one of "greener" synthesis methodologies in synthetic chemistry which can reduce the chemical reaction time and improve the yield and reproducibility of a specific synthesis protocol [25]. Thus, the microwave route has been proved to be a low-cost and energy-saving technique for synthesizing NCs [26–28]. On the other hand, many AuNCs-based nano-probes have been designed to detect metal ions, biological molecules, and temperature [29–34]. However, the nano-probes rely on single "turn-off" or "turn-on" process of fluorescence intensity in visible region. Therefore, the "on − off − on" fluorescent probe is prepared using NIR AuNCs, herein. Resultant AuNCs were synthesized by the microwave-assisted method without using additional reducing agents. This method can form AuNCs rapidly and is suitable for mass production. AuNCs show high stability of NIR fluorescence with λ_{max} 680 nm. Moreover, resultant AuNCs can be used "on − off − on" as NIR fluorescent probe for detecting Cu^{2+} and Vitamin C in aqueous solution and living cells simultaneously.

Experimental section

Chemicals and reagents

Bovine serum albumin (BSA) was purchased from Aldrich (http://www.sigmaaldrich.com). Tetrachloroauric (III) acid ($HAuCl_4$), sodium hydroxide (NaOH) and Vitamin C were analytical grade. The solution of Cu^{2+} was prepared from $Cu(NO_3)_2$. The solutions of other metal ions were prepared from their nitrate, acetate, or chloride salts, and freshly prepared before using. These reagents were purchased from Sinopharm Chemical Reagent Co, Ltd., China (http://www.sinoreagent.com) and used as received without further purification.

The synthesis of Au nanoclusters

Au nanoclusters (AuNCs) were synthesized through a one-step microwave-assisted treatment. In the typical process, BSA (10 mg) and $HAuCl_4$ (0.5 mL, 50 mmol·L^{-1}) were dissolved in 4.5 mL aqueous solution under magnetic stirring. Then, 15 μL NaOH (1 mol·L^{-1}) solution was introduced and the mixture was heated in a microwave oven (800 W, Midea, China) for 20 min. The color of the solution changed from light yellow to deep brown. The purification of resultant BSA − AuNCs was centrifuging at 1100 g to remove excess BSA. The above purification process was repeated three times, followed by collecting the precipitate on the bottom. Then resultant BSA–AuNCs was freeze-dried for further use.

Selective Cu^{2+} detection using the BSA − AuNCs

$Cu(NO_3)_2$ was used for the study of Cu^{2+} detection. Various Cu^{2+} concentrations from 10^{-3} to 10^{-9} M were prepared. For the sensor study, 0.5 ml of aqueous solution of resultant BSA − AuNCs (5 mg·mL^{-1}) and 2.5 ml of Cu^{2+} solution with different concentrations were mixed, and equilibrated for 1 min before the spectral measurements. To check the selectivity cations of this sensor, we carried out interference tests with Mn^{2+}, Cr^{3+}, CrO_4^{2-}, Mg^{2+}, Ca^{2+}, Na^+, Ba^{2+}, K^+, Co^{2+}, Ni^{2+}, Fe^{3+} and Zn^{2+}. The operation was exactly same conditions that were used for the detection of Cu^{2+}. The fluorescence measurements were carried out upon excitation at 500 nm.

Fluorescence "off−on" assay for vitamin C

In order to investigate the fluorescence detection of Vitamin C (VC), we measured the response of the above quenched fluorescence of the BSA − AuNCs with changing the concentration of VC. $Cu(NO_3)_2$ aqueous solution (1.0 mM, 0.2 mL) was firstly mixed with a dispersion of BSA − AuNCs (3 mg·mL^{-1}, 1.8 mL) for 10 min. After different concentrations of VC were added and equilibrated for 5 min, the fluorescence measurements were carried out upon excitation at 500 nm.

Cellular imaging

HeLa cells (2^{10} cells per mL) were cultured in Dulbecco's modified Eagle's medium supplemented with 10% fetal

bovine serum and 1% penicillin–streptomycin (DMEM) using a 96-well plate. Suspensions (10 μg·mL^{-1}) of the BSA − AuNCs from the stock solution were prepared with Dulbecco's phosphate buffer saline (DPBS). After sonication for 10 min to ensure complete dispersion, an aliquot (typically 0.01 mL) of the suspension was added to the well of a chamber slide containing the cells cultured for 4 h. The chamber slide was then incubated at 37 °C in a CO_2 incubator for 4 h for the BSA − AuNCs uptake (only 1.5 mg of BSA − AuNCs to 150 mL of culture medium (10^5 cells) was added). Prior to the fixation of the cells on the slide for inspection with a confocal fluorescence microscope, the excess BSA − AuNCs were removed by washing 3 times with warm DPBS.

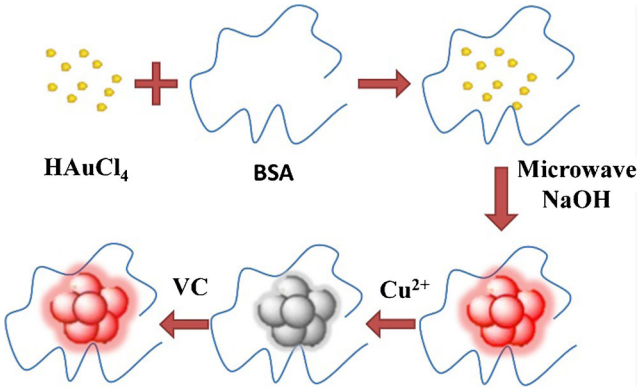

Scheme 1 Synthesis procedure of BSA − AuNCs by microwave-assistant method and their applications as "on − off − on" fluorescent probe for detecting Cu^{2+} and VC

Characterization methods

Steady state fluorescence spectra were measured by a Fluorescence Lifetime Spectrometers (PTI, USA). UV − Vis optical spectra were recorded with a TU − 1991 UV − Vis spectrophotometer. The morphology and size of BSA − AuNCs were observed with a transmission electron microscope (TEM, JEM − 2100) operating at 200 kV. The VG ESCALAB MKII spectrometer with Mg K_α excitation (1253.6 eV) was used to collect the X−ray photoelectron spectroscopy (XPS) data. Fourier transform infrared (FTIR) spectra were recorded with a Nicolet 6700 FTIR spectrophotometer at wavenumbers ranging from 500 to 4000 cm^{-1}. The confocal microscopy images were collected by a confocal fluorescence microscope (FV1000, Olympus).

Results and discussion

Choice of materials and methods

The advantages of microwave-assisted techniques are uniform heating, rapid reaction, low energy of consumption, cost-effectiveness, and environmentally friendly feature [35–38]. Herein, the successful preparation of BSA − AuNCs was carried out by a low-cost and energy-saving microwave-assisted method as shown in Scheme 1. To protect the structure of BSA, ensue efficient absorption of the microwave energy, and to warrant rapid microwave heating, water was selected as the reaction medium due to its favorable di electric constant and dielectric loss constant [37]. In this study, microwave irradiation for 20 min was temporarily paused to prevent the reaction mixture from overheating. In this process, nanoclusters were formed after mixing BSA and $HAuCl_4$ without using additional reducing agents in aqueous solution. BSA played a role both as stabilizing agent and reducing agent in the preparation, based on its capability to sequester and reduce Au precursors in situ. If using other ligands (ascorbic acid, or cystein, or casein), it is hard to observe the fluorescence as shown in Fig. S1. AuNCs show high stability of near-infrared (NIR) fluorescence with a λ_{max} of 675 nm. Moreover, BSA − AuNCs can be used "on − off − on" NIR fluorescent probe for detecting Cu^{2+} and VC in aqueous solution and living cells simultaneously. Table S1 showed the comparison of different probes for determination of Cu^{2+}. It is apparent the AuNCs can act as fluorescent probes for detection of Cu^{2+} with highly selective and sensitive.

The characterization of BSA − AuNCs

The optical properties of resultant BSA − AuNCs were investigated using UV − vis absorption and fluorescence spectrophotometer. As shown in Fig. 1, BSA − AuNCs have an absorption band at around 280 nm, which is assigned to the absorption of BSA [39]. Moreover, there was the absence of absorption at 520 nm, which corresponded to the surface plasmon resonance absorption of large Au nanoparticles (size >2 nm), had informed the presence of oxidation states of Au on the surface which failed to provide free electrons, and this result was consistent with previously reported fluorescent Au nanoparticles [40]. A strong fluorescence center on 675 nm in the near-infrared region is observed from our BSA − AuNCs in aqueous solution upon excitation at 500 nm (Fig. 1) and the full width at half maximum was around 90 nm that covered the red to NIR region, which made resultant BSA − AuNCs useful markers for imaging in the 650 ~ 800 nm range, where tissue and blood optical properties are highly favorable for biomedical imaging. The fluorescence quantum yield of resultant BSA − AuNCs reached up to 6.0% using Rodamine 6G (QY 0.95 in ethanol) as the standard. By our knowledge, this value is thus comparable to that of previously reported NIR NCs [41]. In addition, microwave-assisted method is facile and suitable for mass production. About 50 mL of BSA − AuNCs were produced which showed brown in room

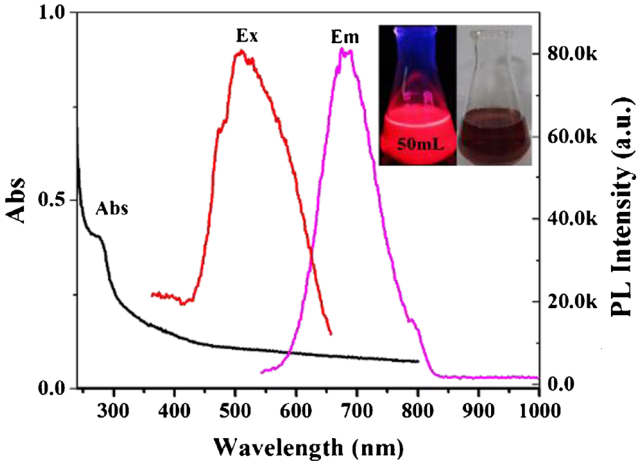

Fig. 1 UV − Vis absorption, excitation (Ex) and emission (Em) spectra of BSA − AuNCs; Inset: the photographs of BSA − AuNCs under visible (right) and 365 nm UV (left) light

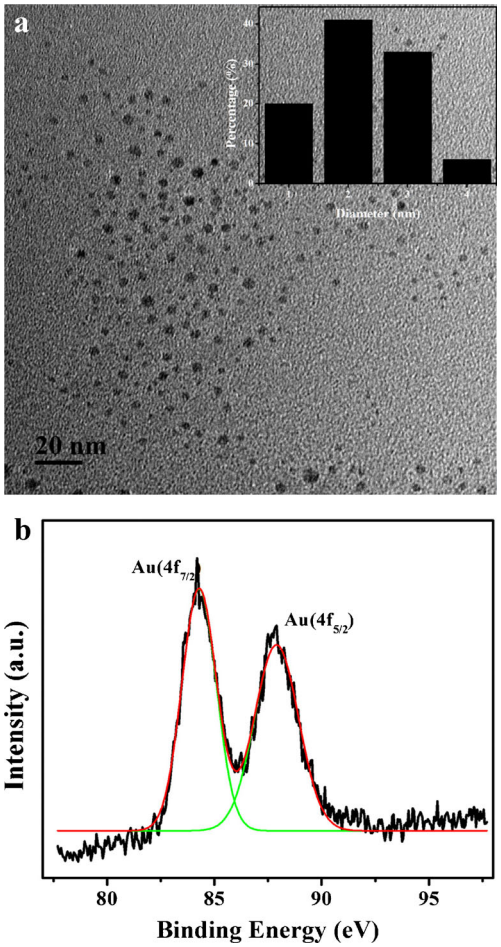

Fig. 2 a, TEM image and (inset) histograms of size distribution of BSA − AuNCs; b, XPS spectra of Au peaks of BSA – AuNCs

light and gave off strong red fluorescence under UV light irradiation (inset of Fig. 1).

Transmission electron microscopy (TEM) was collected to examine the morphology and size of BSA − AuNCs. As shown in Fig. 2a, TEM image showed that resultant BSA − AuNCs were uniform nanoparticles with mean size of approximately 2.8 ± 0.5 nm and presented a nearly spherical shape. In addition, there was no apparent aggregation which indicated BSA − AuNCs had a good dispersion in aqueous solution (inset of Fig. 1). X − ray photoelectron spectroscopy (XPS) was performed to confirm the elemental compositions and chemical bonds of BSA − AuNCs. The XPS survey spectra presented that fluorescent BSA − AuNCs were mainly composed of Au, S, C, N, O elements (Fig. S2a). As presented in Fig. S2b, the high resolution spectra of C 1 s were deconvoluted into three unit moieties, corresponding to C=C/C−C at 284.3 eV, C−N at 285.1 eV, C=O/C=N at 287.4 eV, respectively [42]. Besides, the high resolution XPS spectra of N1s (Fig. S2c) and O1s (Fig. S2d) further confirmed the existing of C−N/N−H and C−OH/C−O−C (532.2 eV) in BSA − AuNCs [43]. These results demonstrated that there are amount of hydrophilic groups on the surface of BSA − AuNCs. Thus these functional groups would improve NCs' solubility and stability in aqueous solution. As presented in Fig. 2b, two intense peaks were observed at 84.2 and 87.8 eV, which were assigned to the $4f_{7/2}$ and $4f_{5/2}$ features of Au(0). The best fit of the data indicates that the BSA − Au NCs consist of approximately 5.2% of Au(I) and 94.8% of metallic Au(0). The existence of a small amount of Au(I) on the surface can help to enhance the stability and QYs of AuNCs [44].

Fourier transform infrared (FTIR) spectroscopy has been used to monitor the changes in the secondary structures of the BSA. Fig. S3 shows the FTIR spectra of the BSA and the BSA − AuNCs. The protein amide I vibration in the region of 1600–1700 cm^{-1} (mainly CO stretch) and the amide II vibration in the region of 1480–1575 cm^{-1} (C–N stretch coupled with N–H bending) are closely related to the secondary structures of the proteins [45]. A shift of the amide I band from 1654 cm^{-1} to a lower wavenumber band (1649 cm^{-1}) was observed, which suggests the possible changes in the secondary structure of BSA when conjugated with the AuNCs [46]. A similar result was observed in the Circular dichroism (CD) spectra of Fig. S4. These results implied that decomposition and intermolecular cyclization reactions took place during the generative process of AuNCs. Besides, BSA, as protective layer on the surface of AuNCs can improve their solubility and stability due to the 17 disulfide bonds and 1 free cysteine [47], which had been widely used in the synthesis of fluorescent NCs [48].

Microwave-assistant synthesis is a rapid reaction, thus controlling experiment conditions becomes highly important, especially reaction time. At the beginning, there was no fluorescence emission. After adding microwave for 1 min, the fluorescence appeared with characteristic peak at 665 nm and spanning the wavelength range 580 ~ 800 nm. With extending the reaction time, the fluorescence characteristic peak slowly

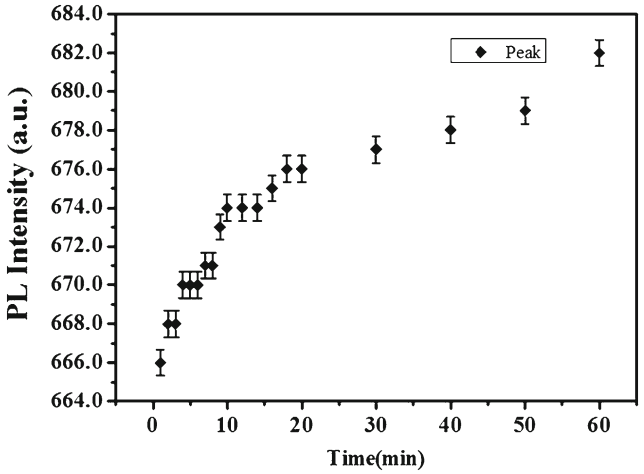

Fig. 3 The fluorescent peaks of resultant BSA − AuNCs with various microwave time

shifted long-wavelength. Similar to quantum dots, the size dependent emission of NCs had been reported from visible red to NIR due to quantum size effect [9, 49]. Thus, we argue that the red-shift of BSA − AuNCs with extending the reaction time resulted from changing the size. When the reaction time was up to 30 min, the fluorescence intensity reached up to 677 nm as shown in Fig. 3. Further increasing the reaction time, the fluorescence emission of AuNCs continued red shift very slow and the fluorescence almost no changed at the reaction time up to 60 min (Fig. S5). Because pH affects the protein structure, it is considered a crucial factor in the formation of BSA–Au NCs [50]. Only at high pH, the NIR fluorescence of AuNCs appeared and formed optimal fluorescence intensity of the BSA − AuNCs at pH 12 (Fig. S6). This was mainly because of an increase in the reduction capability of BSA. The tyrosine residue of BSA is responsible for reducing Au^{3+} to Au^{0} at pH levels greater than the pKa of tyrosine (approximately 10). At low pH levels (<6.0), BSA did not exert a reducing effect on the formation of BSA–AuNCs. At high pH levels (>12.0), a high NaOH concentration quenched the fluorescence intensity of BSA–Au NCs. Fig. S6 also demonstrated that the ratio of BSA and Au precursor would influence on appearing NIR fluorescence.

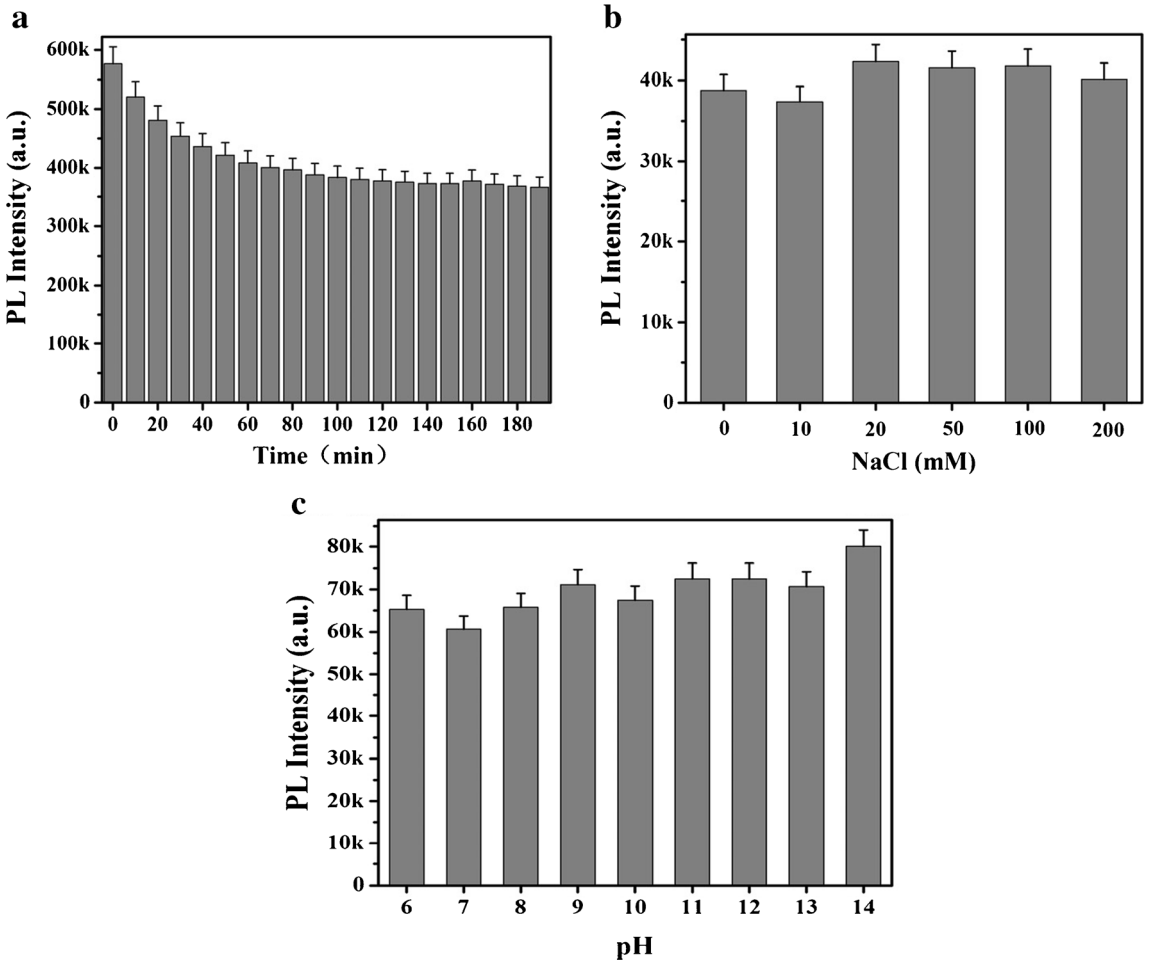

Fig. 4 **a** Histogram of fluorescence intensity (675 nm) of BSA–AuNCs under 450 W Xe lamp irradiation for different time; **b** Histogram of fluorescence (675 nm) of resultant BSA–AuNCs in NaCl solution with various concentrations; **c** Histogram of fluorescence (675 nm) of resultant BSA–AuNCs in various pH values

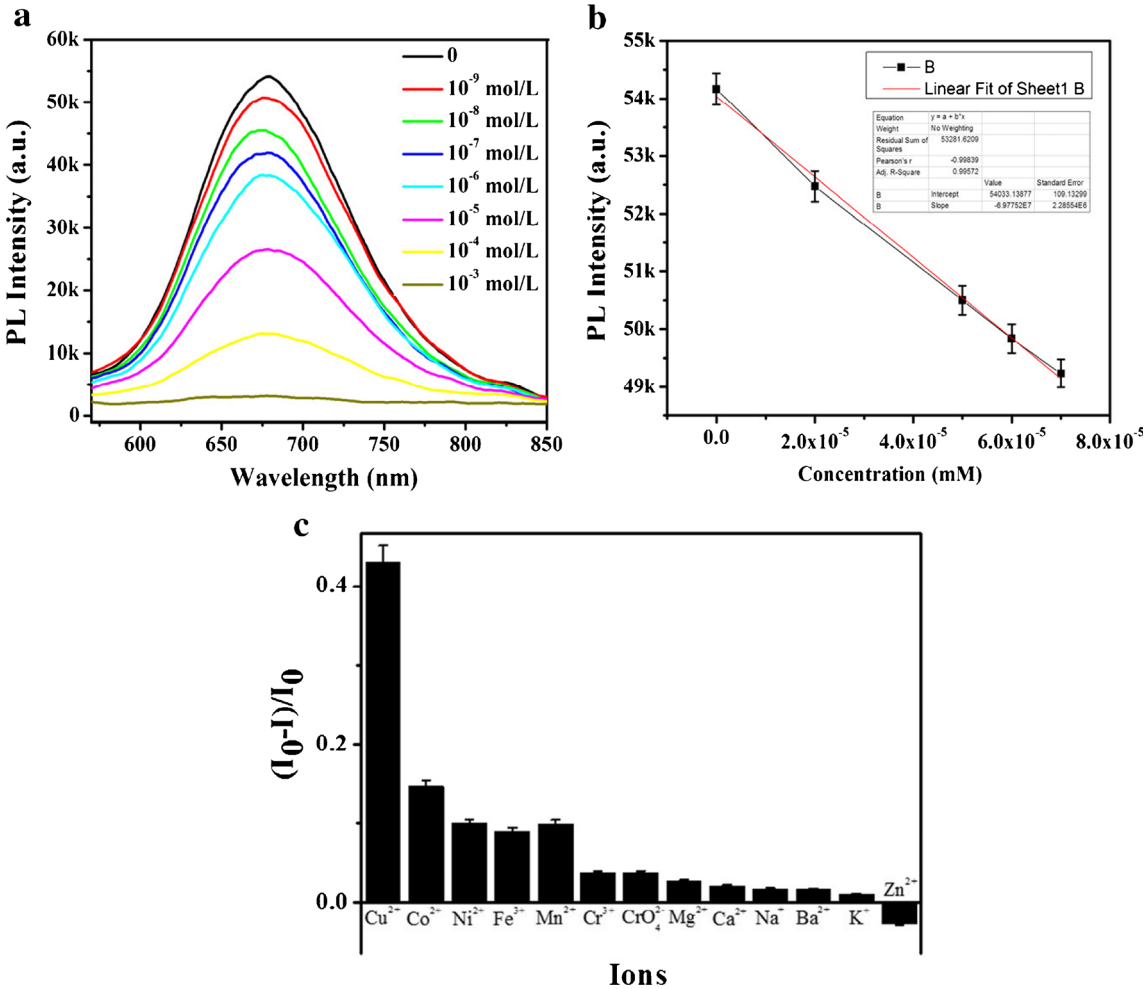

Fig. 5 **a** Fluorescence quenching of BSA − AuNCs upon adding different concentration of Cu^{2+} ions (0 ~ 1 mM), upon excitation at 500 nm; **b** plot of fluorescence intensity (675 nm) of resultant BSA − AuNCs vs various amount of Cu^{2+} ions; **c** Histogram of fluorescence intensity (675 nm) of BSA − AuNCs after adding different metal ions

According to previously reported fluorescent nanomaterials, the stability of them was an important element to evaluate their practical applications [51]. Consequently, the stability of resultant BSA–AuNCs needed to be measured before their application. Although some fluorescent nanomaterials (organic dyes, proteins and quantum dots) show high quantum yield, their applications would be limited by poor stability [52]. Unlike those fluorescence objects, as-synthesized BSA–AuNCs may broaden bio-applications of luminescent nanomaterials owing to an ultra-stable property. Herein, BSA–AuNCs are exposed under a 450 W xenon (Xe) lamp for various time spans to probe their photo-stability. The fluorescence intensity of Au NCs decrease only slightly, and preserve ~80% of the initial intensity even after 180 min irradiation by 450 W Xe lamp (Fig. 4a and Fig. S7), which has been much more stable than FITC dye or CdTe QDs [53].

Additionally, the fluorescence intensity of BSA–AuNCs had no obvious change with increasing the concentration of NaCl solution (Fig. 4b and Fig. S8). Even when the concentration was up to physiological ionic strength (NaCl, 200 mM), the fluorescence intensity still remained constant. Thus, salt resistance of BSA–AuNCs was a significant factor to achieve their bio-applications. Moreover, in the relevant pH range of 6–14, the fluorescence intensity of BSA–AuNCs have tiny change as shown in Fig. 4c, indicating that these BSA–AuNCs possess a relative high pH-stability (Fig. S9). In a word, the NIR AuNCs with good photo-, pH- and ions-stability in this article are particular appropriate for practical applications. We argue the high stability of resultant AuNCs caused by surface protection of BSA. The AuNCs formed in the BSA solution have been stabilized by a combination of Au − S bonding with the protein (via the 35 Cys residues in BSA), and the steric protection due to the bulkiness of the protein [54]. The high stability of BSA–AuNCs would greatly facilitate their use in in vitro and in vivo bioimaging applications [48].

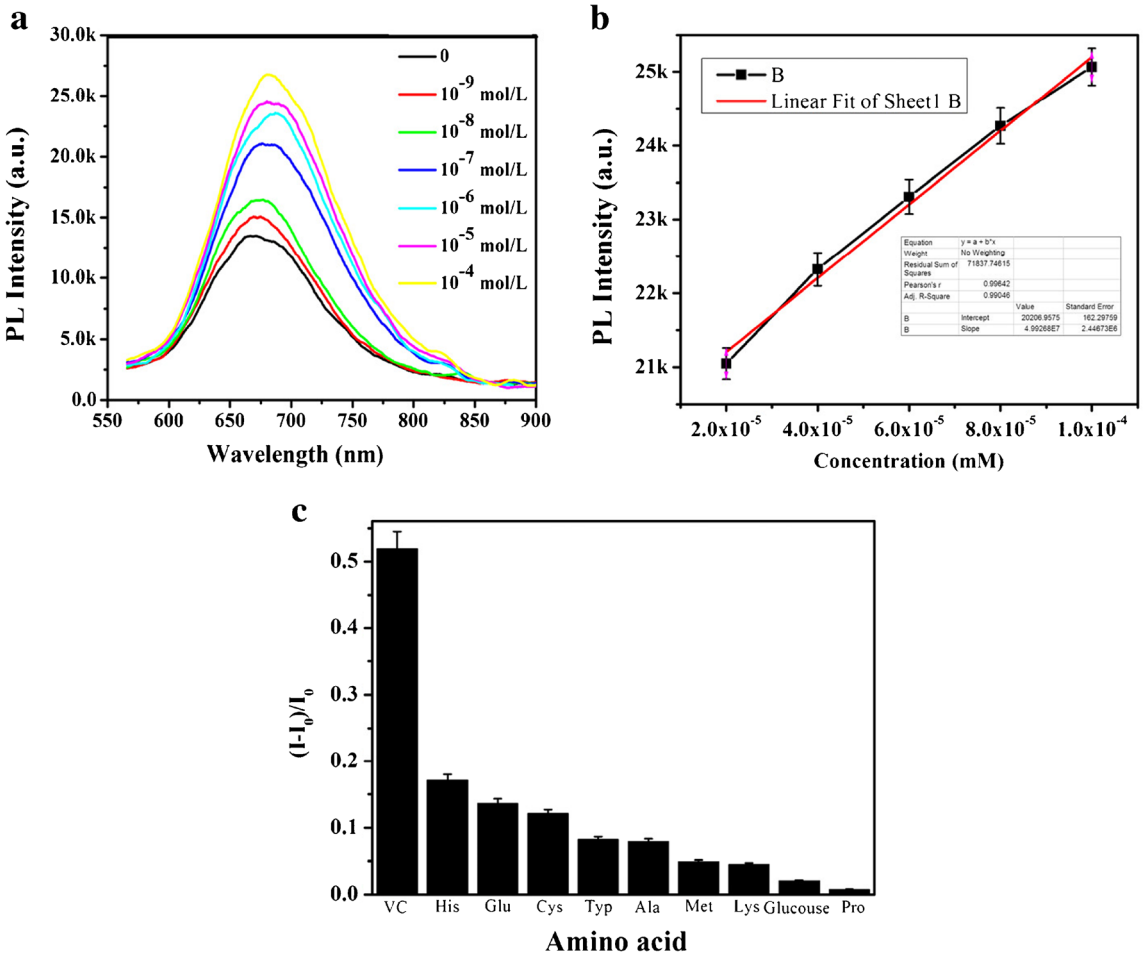

Fig. 6 **a** fluorescence spectra of BSA − AuNC/Cu^{2+} complex upon adding different concentration of VC, upon excitation at 500 nm; **b** plot of fluorescence intensity (675 nm) of resultant BSA − AuNC/Cu^{2+} complex vs various amount of VC; **c** Histogram of fluorescence intensity (675 nm) of BSA − AuNC/Cu^{2+} complex after adding various biomolecules

The on-off-on probe for Cu^{2+} and vitamin C

Copper is not only one of essential elements for animals and human beings with existing in many proteins and enzymes, but also widely used in industry and medicines. The leak of copper ions (Cu^{2+}) will lead to the serious health problems, for example, memory impairment, leukotrichia. However, too much intake of Cu^{2+} can cause the gastrointestinal disorders. Thus, it is important to sensitively analyze the concentration of Cu^{2+}. BSA–AuNCs can be used as a highly sensitive and selective fluorescence probe for Cu^{2+} detection due to the present of BSA on the surface. BSA has a much-stronger affinity toward Cu^{2+}, which caused the aggregation of NCs (seeing the TEM image of Fig. S10a). This sensing mechanism based on aggregation-induced fluorescence quenching had been widely adopted for NCs as probe to determine metal ions [7, 38, 55, 56]. So with this fluorescence active, water soluble NCs in hands, we then investigated their ability as probe in selective metal Cu^{2+} detection. It was found that the fluorescence of BSA − AuNCs was efficiently quenched by the Cu^{2+} ions. The fluorescence spectra displayed a gradual decrease in emission intensity with increasing the concentration of Cu^{2+} (Fig. 5a). The fluorescence intensity of BSA − AuNCs decreased to about 10% of the original fluorescence intensity after the adding Cu^{2+} ions (100 μM) as shown in Fig. 5b, indicating that the Cu^{2+} ions can effectively quench the fluorescence of BSA − AuNCs. The sensing mechanism can be ascribed to electron or energy transfer between Cu^{2+} ions and BSA − AuNCs. The limit of detection (LOD) is estimated to be 10 nM, which is much lower than the maximum safety level of Cu^{2+} (20 μM) in drinking water defined by the US Environmental Protection Agency (EPA).

The selectivity of the assay was investigated (Fig. 5c). A number of metal ions was tested (Cu^{2+}, Mn^{2+}, Cr^{3+}, CrO_4^{2-}, Mg^{2+}, Ca^{2+}, Na^{+}, Ba^{2+}, K^{+}, Ni^{2+}, Co^{2+}, Fe^{3+} and Zn^{2+}) under the same experimental conditions. The results clearly show that little emission intensity changes were observed in the presence of these interference metal ions (Fig. 5c and Fig. S11), which demonstrates that the assay method is highly selective detection of Cu^{2+}. Literature reports have shown that

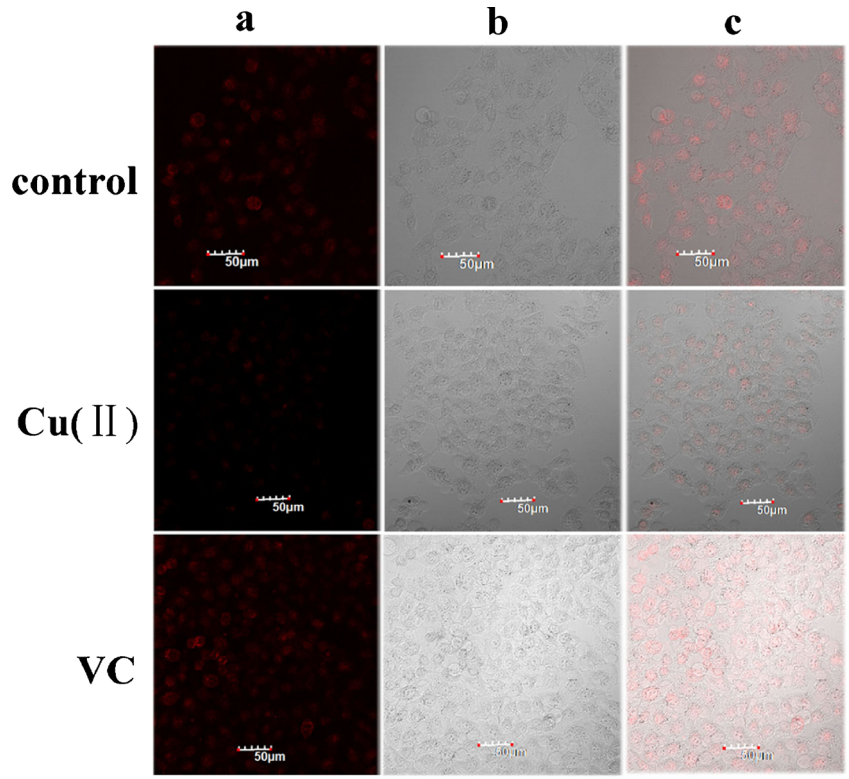

Fig. 7 **a** Confocal fluorescent images, **b** bright field, and **c** overlay images of Hela cells with incubated with BSA − AuNCs, BSA − AuNC/Cu^{2+} complex and adding VC

there are metallophilic interactions between the d^{10} centers of Hg^{2+} and Au^{+} [50]. Thus, the presence of Hg^{2+} does interfere with the detection of Cu^{2+}. However, it was reported that the interference can be removed by the addition of a proper amount of Sn^{2+} [57].

The quenched fluorescence of BSA − AuNCs by Cu^{2+} ions can be basically recovered by adding Vitamin C (VC). As shown in Fig. 6a, the fluorescence intensity of BSA − AuNC/Cu^{2+} complex increase upon adding the concentrations of VC. The reason is that VC competitively binds with Cu^{2+} ions in the BSA − AuNC/Cu^{2+} complex by forming a more stable complex Cu^{2+}/VC. The interaction between Cu^{2+} ions and BSA − AuNCs would be weakened by the competitive coordination of the imidazole group, and part of Cu^{2+} ions can be taken away from the BSA − AuNC/Cu^{2+} complex (seeing the TEM image of Fig. S10b), then the fluorescence of BSA − AuNCs would be dramatically enhanced. This result indicates that the response of BSA − AuNC/Cu^{2+} complex by VC is rapid and stable, implying a promising application in a fast sensing of VC without strict time control. Moreover, the linear relationship between the fluorescence intensity enhancement and the concentration of VC was observed in Fig. 6b. The limit of detection (LOD) is estimated to be 24 nM. This fact demonstrated that the as designed biosensor possessed excellent selectivity toward VC determination. The fluorescence responses of BSA − AuNC/Cu^{2+} complex were also investigated in the presence of various biomolecules (VC, cysteine (Cys), histidine (His), glutamic acid (Glu), tryptophan (Typ), methionine (Met), glucose, lysine (Lys), alanine (Ala), and proline (Pro)) under the same experimental conditions. The results indicated that the tested amino acids have less influence on the VC determination by using the NIR BSA − AuNC/Cu^{2+} complex as nanoprobes (Fig. 6c and Fig. S12).

BSA − AuNCs showed water-dispersion, high stability, and good biocompatibility and NIR emission. Especially, the NIR fluorescence has advantages in biological imaging due to relatively high transparency and low auto-fluorescence in living tissues. Thus, to evaluate whether the NIR AuNCs-based fluorescent probe is applicable to biological fields, HeLa cells are used as the model to explore the possibility of using NIR AuNCs for on-off-on detection of Cu^{2+} and VC in living cells. Before that, toxicity is a major factor that needs consideration in the design of an intracellular sensor system for subsequent biological applications. To evaluate the cytotoxicity of the BSA − AuNCs, a thiazolyl blue tetrazolium bromide (MTT) assay was conducted on cells loaded with BSA − AuNCs. As shown in Fig. S13, the viability of HeLa cells remained above 80% following incubation with the BSA − AuNCs, even at a concentration of 100 μg/mL for 24 h, considerably more forcing conditions than those used for cell incubation and imaging. A similar result was observed in the MTT assay of 293 T cells (Fig. S14). These results indicate the NIR BSA − AuNCs are biocompatible and low toxicity.

After incubating, both the HeLa and MC3T3 − E1 cells exhibit intense red fluorescence in the cytosol irradiated by

450 nm and the cells maintained their normal morphology, thus indicating the good biocompatibility of NIR BSA − AuNCs (Fig. 7 and Fig. S15). Upon adding Cu^{2+} solution (10–100 μM in MC3T3 − E1 cells and 100 μM in HeLa cells) at room temperature, the red fluorescence in cells would decrease (Fig. 7 and Fig. S15), which was consistent with the changes in the fluorescence spectra observed in aqueous solution in presence of Cu^{2+}. However, adding the VC, the NIR fluorescence would be recovered (Fig. 7). These results demonstrate that this system can readily internalize into the cytoplasm of the cell and work as on-off-on nanosensor in living cells. Thus, resultant NIR BSA − AuNCs can be used "on − off − on" NIR fluorescent probe for detecting Cu^{2+} and VC in aqueous solution and living cells simultaneously.

Conclusions

In summary, NIR AuNCs with BSA worked both as stabilizing agent and reducing agent were synthesized by a facile and rapid microwave-assisted method. BSA − AuNCs showed NIR fluorescence, high quantum yield and small size. Moreover, resultant BSA − AuNCs showed the excellent salt-, photo- and pH- stability. The NIR fluorescence of BSA − AuNCs would be quenched by Cu^{2+} ions and quenched fluorescence is recovered by Vitamin C (VC). Thus, NIR BSA − AuNCs can be utilized for "on − off − on" fluorescent probe for detecting Cu^{2+} and VC in aqueous solution simultaneously through the fluorescence quenching and recovery processes, respectively. Furthermore, utilization of resultant "on − off − on" fluorescent probe for monitoring Cu^{2+} and VC in living cells has been successfully demonstrated. Thus, these BSA − AuNCs with facile preparation, water-dispersion, high stability, good biocompatibility and NIR emission, hold great promise as an alternative to conventional fluorescence probes for biolabeling, sensing and other applications.

Acknowledgements This work was supported by the National Natural Science Foundation of China (No. 51503085), the Natural Science Foundation of Jiangsu Province, China (No. BK20140157), open project of state key laboratory of supramolecular structure and materials (sklssm201621), Provincial Institution Promotion Plan (2015024-3), Public Health Research Center at Jiangnan University (No.JUPH201506), 2015 postgraduate practice innovation project of ordinary college in Jiangsu (SJLX15_0552).

Compliance with ethical standards The authors have no competing interests.

References

1. Guan WJ, Zhou WJ, Lu J, Lu C (2015) Luminescent films for chemo- and biosensing. Chem Soc Rev 44:6981–7009
2. Han JS, Zhang X, Zhou YB, Ning Y, Wu J, Liang S, Sun HC, Zhang H, Yang B (2012) Fabrication of CdTe nanoparticles-based superparticles for an improved detection of Cu^{2+} and Ag^{+}. J Mater Chem 22:2679–2686
3. Yang XD, Shen BW, Jiang YN, Zhao ZX, Wang CX, Ma C, Yang B, Lin Q (2013) A novel fluorescent polymer brushes film as a device for ultrasensitive detection of TNT. J Mater Chem A 1: 1201–1206
4. Ma Q, Su XG (2011) Recent advances and applications in QDs-based sensors. Analyst 136:4883–4893
5. Jiang YN, Yang XD, Ma C, Wang CX, Li H, Dong FX, Zhai XM, Yu K, Lin Q, Yang B (2010) Photoluminescent smart hydrogels with reversible and linear Thermoresponses. Small 6:2673–2677
6. Wang CX, Xu ZZ, Cheng H, Lin HH, Humphrey MG, Zhang C (2015) A hydrothermal route to water-stable luminescent carbon dots as nanosensors for pH and temperature. Carbon 82:87–95
7. Wang CX, Cheng H, Huang YJ, Xu ZZ, Lin HH, Zhang C (2015) Facile sonochemical synthesis of pH-responsive copper nanoclusters for selective and sensitive detection of Pb^{2+} in living cells. Analyst 140:5634–5639
8. Guo ZQ, Park SK, Yoon JY, Shin I (2014) Recent progress in the development of near-infrared fluorescent probes for bioimaging applications. Chem Soc Rev 43:16–29
9. Wang CX, Wang Y, Xu L, Zhang D, Liu MX, Li XW, Sun HC, Lin Q, Yang B (2012) Facile aqueous-phase synthesis of biocompatible and fluorescent Ag_2S nanoclusters for bioimaging: tunable photoluminescence from red to near infrared. Small 8:3137–3142
10. Du JJ, Yu CM, Pan DC, Li JM, Chen W, Yan M, Segura T, Lu YF (2010) Quantum-dot-decorated robust Transductable bioluminescent Nanocapsules. J Am Chem Soc 132:12780–12781
11. Wang CX, Xu L, Xu XW, Cheng H, Sun HC, Lin Q, Zhang C (2014) Near infrared Ag/Au alloy nanoclusters: tunable photoluminescence and cellular imaging. J Colloid Interface Sci 416:274–279
12. Goswami N, Giri A, Kar S, Bootharaju MS, John R, Xavier PL, Pradeep T, Pal SK (2012) Protein-directed synthesis of NIR-emitting, tunable HgS quantum dots and their applications in metal-ion sensing. Small 8:3175–3184
13. Xia YS, Song L, Zhu CQ (2011) Turn-on and near-infrared fluorescent sensing for 2,4,6-trinitrotoluene based on hybrid (gold nanorod)-(quantum dots) assembly. Anal Chem 83:1401–1407
14. Lu YZ, Chen W (2012) Sub-nanometre sized metal clusters: from synthetic challenges to the unique property discoveries. Chem Soc Rev 41:3594–3623
15. Shang L, Dong SJ, Nienhaus GU (2011) Ultra-small fluorescent metal nanoclusters: synthesis and biological applications. Nano Today 6:401–418
16. Zhang LB, Wang EK (2014) Metal nanoclusters: new fluorescent probes for sensors and bioimaging. Nano Today 9:132–157
17. Wang CX, Wang Y, Xu Y, Shi XD, Li XW, Xu XW, Sun HC, Yang B, Lin Q (2013) A galvanic replacement route to prepare strongly fluorescent and highly stable gold Nanodots for cellular imaging. Small 9:413–420
18. Wang CX, Cheng H, Sun YQ, Lin Q, Zhang C (2015) Rapid sonochemical synthesis of luminescent and paramagnetic copper nanoclusters for bimodal bioimaging. Chem NanoMat 1:27–31
19. Li G, Jin RC (2013) Atomically precise gold nanoclusters as new model catalysts. Acc Chem Res 46:1749–1758
20. Zheng J, Zhou C, Yu MX, Liu JB (2012) Different sized luminescent gold nanoparticles. Nanoscale 4:4073–4083
21. Shang YC, Huang CC, Chen WY, Chen PC, Chang HT (2012) Fluorescent gold and silver nanoclusters for analysis of biopolymers and cell imaging. J Mater Chem 22:12972–12982
22. Chen LY, Wang CW, Yuan ZQ, Chang HT (2015) Fluorescent gold nanoclusters: recent advances in sensing and imaging. Anal Chem 87:216–229

23. Zheng J, Petty JT, Dickson RM (2003) High quantum yield blue emission from water-soluble Au_8 Nanodots. J Am Chem Soc 125: 7780–7781
24. Chen Y, Zhou HP, Wang Y, Li WY, Chen J, Lin Q, Yu C (2013) Substrate hydrolysis triggered formation of fluorescent gold nanoclusters – a new platform for the sensing of enzyme activity. Chem Commun 49:9821–9823
25. Bilecka I, Niederberger M (2010) Microwave chemistry for inorganic nanomaterials synthesis. Nanoscale 2:1358–1374
26. Hsu NY, Lin YW (2016) Microwave-assisted synthesis of bovine serum albumin–gold nanoclusters and their fluorescence-quenched sensing of Hg^{2+} ions. New J Chem 40:1155–1161
27. Raut S, Rich R, Fudala R, Butler S, Kokate R, Gryczynski Z, Luchowskic R, Gryczynski I (2014) Resonance energy transfer between fluorescent BSA protected Au nanoclusters and organic fluorophores. Nanoscale 6:385–391
28. Gu Y, Li N, Gao M, Wang Z, Xiao D, Li Y, Jia H, He H (2015) Microwave-assisted synthesis of BSA-modified silver nanoparticles as a selective fluorescent probe for detection and cellular imaging of cadmium(II). Microchim Acta 182:1255–1261
29. Chen Y, Wang Y, Wang CX, Li WY, Zhou HP, Jiao HP, Lin Q, Yu C (2013) Papain-directed synthesis of luminescent gold nanoclusters and the sensitive detection of Cu^{2+}. J Colloid Interface Sci 396:63–68
30. Chen Y, Li WY, Wang Y, Yang XD, Chen J, Jiang YN, Yu C, Lin Q (2014) Cysteine-directed fluorescent gold nanoclusters for the sensing of pyrophosphate and alkaline phosphatase. J Mater Chem C 2: 4080–4085
31. Yang S, Jiang Z, Chen Z, Tong L, Lu J, Wang J (2015) Bovine serum albumin-stabilized gold nanoclusters as a fluorescent probe for determination of ferrous ion in cerebrospinal fluids via the Fenton reaction. Microchim Acta 182:1911–1916
32. Xu S, Yang H, Zhao K, Li J, Mei L, Xie Y, Deng A (2015) Preparation of orange-red fluorescent gold nanoclusters using denatured casein as a reductant and stabilizing agent, and their application to imaging of HeLa cells and for the quantitation of mercury (II). Microchim Acta 182:2577–2584
33. Shang L, Stockmar F, Azadfar N, Nienhaus GU (2013) Intracellular thermometry by using fluorescent gold nanoclusters. Angew Chem Int Ed 52:11154–11157
34. Wang CX, Lin HH, Xu ZZ, Huang YJ, Humphrey MG, Zhang C (2016) Tunable carbon-dot-based dual-emission fluorescent nanohybrids for ratiometric optical thermometry in living cells. ACS Appl Mater Interfaces 8:6621–6628
35. Xu ZZ, Wang CX, Jiang KL, Lin HH, Huang YJ, Zhang C (2015) Microwave-assisted rapid synthesis of amphibious yellow fluorescent carbon dots as a colorimetric nanosensor for Cr(VI). Part Part Syst Charact 32:1058–1062
36. Liu Y, Tian GF, He XW, Li WY, Zhang YK (2016) Microwave-assisted one-step rapid synthesis of near-infrared gold nanoclusters for NIRF/CT dual-modal bioimaging. J Mater Chem B 4:1276–1283
37. Yan L, Cai YQ, Zheng BZ, Yuan HY, Guo Y, Xiao D, Choi MMF (2012) Microwave-assisted synthesis of BSA-stabilized and HSA-protected gold nanoclusters with red emission. J Mater Chem 22: 1000–1005
38. Raut S, Chi R, Rich R, Shumilov D, Gryczynski Z, Gryczynski I (2013) Polarization properties of fluorescent BSA protected Au_{25} nanoclusters. Nanoscale 5:3441–3446
39. Wang CX, Cheng H, Sun YQ, Xu ZZ, Lin HH, Lin Q, Zhang C (2015) Nanoclusters prepared from a silver/gold alloy as a fluorescent probe for selective and sensitive determination of lead(II). Microchim Acta 182:695–701
40. Li J, Wu J, Zhang X, Liu Y, Zhou D, Sun HZ, Zhang H, Yang B (2011) Controllable synthesis of stable urchin-like gold nanoparticles using hydroquinone to tune the reactivity of gold chloride. J Phys Chem C 115:3630–3637
41. Udayabhaskararao T, Sun Y, Goswami N, Samir KP, Balasubramanian K, Pradeep T (2012) Ag_7Au_6: a 13-atom alloy quantum cluster. Angew Chem Int Ed 51:2155–2159
42. Qu SN, Zhou D, Li D, Ji WY, Jing PT, Han D, Liu L, Zeng HB, Shen DZ (2016) Toward efficient Orange emissive carbon Nanodots through conjugated sp^2-domain controlling and surface charges engineering. Adv Mater 28:3516–3521
43. Zhou J, Yang Y, Zhang CY (2013) A low-temperature solid-phase method to synthesize highly fluorescent carbon nitride dots with tunable emission. Chem Commun 49:8605–8607
44. Chen PC, Chiang CK, Chang HT (2013) Synthesis of fluorescent BSA–Au NCs for the detection of Hg^{2+} ions. J Nanopart Res 15: 1336–1345
45. Ding H, Yu SB, Wei JS, Xiong HM (2016) Full-color light-emitting carbon dots with a surface-state-controlled luminescence mechanism. ACS Nano 10:484–491
46. Hu DH, Sheng ZH, Gong P, Zhang PF, Cai LT (2010) Highly selective fluorescent sensors for Hg^{2+} based on bovine serum albumin-capped gold nanoclusters. Analyst 135:1411–1416
47. Mathew A, Sajanlal PR, Pradeep T (2011) A fifteen atom silver cluster confined in bovine serum albumin. J Mater Chem 21: 11205–11212
48. Xie JP, Zheng YG, Ying JY (2009) Protein-directed synthesis of highly fluorescent gold nanoclusters. J Am Chem Soc 131:888–889
49. Richards C, Choi S, Hsiang JC, Antoku Y, Vosch T, Bongiorno A, Tzeng YL, Dickson RM (2008) Oligonucleotide-stabilized Ag Nanocluster fluorophores. J Am Chem Soc 130:5038–5039
50. Shang L, Nienhaus GU (2012) Gold nanoclusters as novel optical probes for in vitro and in vivo fluorescence imaging. Biophys Rev 4:313–322
51. Chen YN, Chen PC, Wang CX, Lin YS, Ou CM, Ho LC, Chang HT (2014) One-pot synthesis of fluorescent BSA–Ce/Au nanoclusters as ratiometric pH probes. Chem Commun 50:8571–8574
52. Unnikrishnan B, Wei SC, Chiu WJ, Cang JS, Hsu PH, Huang CC (2014) Nitrite ion-induced fluorescence quenching of luminescent BSA-Au25 nanoclusters: mechanism and application. Analyst 139: 2221–2228
53. Cheng H, Wang CX, Xu ZZ, Lin HH, Zhang C (2015) Gold nanoparticle-enhanced near infrared fluorescent nanocomposites for targeted bio-imaging. RSC Adv 5:20–26
54. Lovrić J, Bazzi HS, Cuie Y, Fortin GRA, Winnik FM, Maysinger D (2005) Differences in subcellular distribution and toxicity of green and red emitting CdTe quantum dots. J Mol Med 83:377–385
55. Goswami N, Giri A, Bootharaju MS, Xavier PL, Pradeep T, Pal SK (2011) Copper quantum clusters in protein matrix: potential sensor of Pb^{2+} ion. Anal Chem 83:9676–9680
56. Adhikari A, Banerjee A (2010) Facile synthesis of water-soluble fluorescent silver nanoclusters and HgII sensing. Chem Mater 22: 4364–4371
57. Xie JP, Zheng YG, Ying JY (2010) Highly selective and ultrasensitive detection of Hg2+ based on fluorescence quenching of Au nanoclusters by Hg2 + −Au + interactions. Chem Commun 46: 961–963